Analysis and Validation of Mathematical Morphology Filters for Single-Ended Fault Localization in VSC-HVDC Links

Ashouri, Mani; Silva, Filipe Miguel Faria da; Bak, Claus Leth

Published in:
Electrical Engineering

DOI (link to publication from Publisher):
10.1007/s00202-020-01186-1

Publication date:
2021

Document Version
Accepted author manuscript, peer reviewed version

Noname manuscript No.
(will be inserted by the editor)

Analysis and Validation of Mathematical Morphology Filters for Single-Ended Fault Localization in VSC-HVDC Links

Mani Ashouri[1] · Filipe Faria da Silva[1] · Claus Leth Bak[1]

Received: date / Accepted: date

Abstract Fast and accurate fault detection and localization are important topics in voltage source converter-based high voltage direct current transmission (VSC-HVDC) grids in order to isolate the fault after the first milliseconds of occurrence. Common signal-processing methods used for detecting fault traveling wave (TW) peaks like Fourier, S-transform and Wavelet-based techniques, transform the signal into the frequency domain, requiring complicated computations. In this paper, the application of mathematical morphology (MM)-based filters for detecting and locating faults in VSC-HVDC links are studied. MM-based methods analyze the signal in the time domain and detect the wave peaks accurately. Multiple MM-based filters resulted from basic MM operators are presented and used for TW-based fault study in VSCHVDC grids. Several fault cases are applied to the CIGRE VSC-HVDC model in PSCAD and the MM-based scripts are written in MATLAB. The impact of different size and type of the Structuring Element (SE) on the accuracy of peak detection is analyzed. The results show the accuracy of MM filters for detecting and locating fault transient in VSC-HVDC links. The proposed method gives accurate results for both low-impedance and high-impedance faults.

Keywords Fault Location · Mathematical Morphology · Transient · Traveling Waves · VSC-HVDC

M. Ashouri
Pontoppidanstræde 111, 1-109- 9220 Aalborg Øst- Denmark
Tel.: +45-93562317
E-mail: maa@et.aau.dk
· F. Faria da Silva
E-mail: ffs@et.aau.dk

C. Leth Bak
E-mail: clb@et.aau.dk

[1] Department of Energy Technology, Aalborg University, Aalborg, Denmark

Abbreviations

I_p, I_n	Positive and negative pole currents.
i_0, i_1	Ground and conductor modal currents.
v	Modal velocity.
f	Frequency of cable calculations.
Λ_k	Propagation constant.
d	Determined cable location.
L_t	Total transmission length.
t_i^R, t_i^L	The i^{th} peak arrival time for the right and left side, respectively.
$f(n)$, $g(n)$	Input signal and the structuring element, respectively.
δ_g , $\in_g$	Dilation and erosion fo the structuring element g.
op_g , cl_g	Opening and closing for the structuring element g.
$\Psi(f)$	Morphological median filter for de-noising function f.
$MG(f)$	Morphological gradient for function f.
$MMG(f)$	Multi-resolution morphological gradient for function f.
$SMMG(f)$	Series multi-resolution morphological gradient for function f.

1 Introduction

Fault detection and localization play an important role in the protection and restoration of both high voltage direct current (HVDC) and high voltage alternating current (HVAC) transmission systems [1]. In voltage source converter-based HVDC (VSC-HVDC) links, the IGBT switches are vulnerable to the fault currents and a fast fault detection algorithm is needed for isolating the fault in the shortest possible duration after the fault occurrence [2]. In addition to the fast fault detection, the location of faults must be determined to speed up the repairing process, or in case of multi-terminal links, separate the faulty section from the grid and have a selective protection system. Locating the faults in HVDC systems is different from the embedded impedance-based fault locators in HVAC distance relays . In fact, the impedance-based techniques are not proper for fault detection and localization in HVDC transmission due to zero reactance and low impedance of HVDC transmission links. One of the possible ways of fault localization is using traveling wave (TW)-based techniques to accurately detect and locate the faults in VSC-HVDC links [3]. These methods may use single-ended, double-ended or wide-area measurement [4] techniques for measuring voltage and current data. The main issue in TW-based methods is that detection of the wave heads and second reflections is challenging, particularly for high-impedance faults. In TW-based methods, high-sampling devices are needed to accurately detect fault initial peaks. Additional to the high-sampling devices, the detection of TWs needs fast and robust signal-processing algorithms for accurate initial peak detection.

Generally, the method of using the fault data and the signal-processing method used for processing the fault signals are the main topics in comparing

the literature works in fault location topics. Authors in [1] proposed a single-ended fault location method, based on residual voltage of MM submodule capacitors. The method has advantage of simplicity and no need for additional voltage sources for locating the fault. However, the method only concentrates on short distance DC overhead line (OHL). Application of the proposed method for VSC-HVDC cable transmission is not investigated and considering that a majority of VSC-HVDC links use underground/submarine cables, the method needs extensive tests fer HVDC cable systems. In [5], a directional rate of change of voltage (ROCOV)-based fault detection and localization scheme is proposed. The proposed method uses local measurement system. It detects and locates the fault before the fault current reaches the maximum breakable value and it can detect faults in different locations in an accurate way. However, the method lacks accuracy in detecting high-resistance faults, which is due to using the rate of change of voltage. In other word, due to using voltage derivatives, the method is dependent on the fault loop impedance [6]. Authors in [6] proposed a transient-based pilot protection scheme using the ratio of the transient voltage between two sides of the supplemental inductors, which are installed on the two sides of the transmission section. This principle makes a clear discrimination between internal and external methods. However, transient-based methods are highly sensitive to noise and lead to fail detections in noisy environment. The method highly depends on the system topology. In [7], a TW-based differential protection method is proposed for VSC-HVDC grids. The method defines a ratio between wavelet-based operation and restrain signals, which makes an accurate discrimination between internal and external faults. However, the method needs a communication link between two sides of the transmission section, leading to possible communication delay or data loss. In [8] a fault location method based on modal theory is presented for HVDC cable transmission. The method is based on the fact that the decoupled modes resulted from the cable layer currents, have different velocities in high frequencies and as a result have different arrival times. The method uses one-sided data and only needs the detection of initial peaks without needing to detect the second detection. However, the method lacks accuracy for deep/shallow water cables or in situations that there are multiple joints between cables. In such situations, the modal behaviors will change, leading to malfunction of the method.

There are several proposed methods that utilize different signal-processing techniques to detect the arrival fault waves and the fault location. The most common methods are Fourier transform (FT), Wavelet transform (WT) and Hilbert-Huang transform (HHT) based techniques. Authors in [9] used fast Fourier transform (FFT) for fault location in HVDC transmission. FFT is fast and simple, but it does not give any information regarding the time domain and it is not the best option to give the most accurate results. Authors in [10] and [11], used discrete wavelet transform (DWT) for designing fault localization algorithms for VSC-HVDC and line commutated converter HVDC (LCC-HVDC) links, respectively. DWT gives a combination of time domain and frequency domain information, which is extensively used for fault location

studies in both HVAC and HVDC transmission. However, the given information is a trade-off between the time domain and frequency domain information. It means with more accurate time domain information, less accurate frequency domain information is given. Moreover, DWT needs more complex computations than FFT. Accordingly, DWT does not give the fastest and the most accurate fault location results for VSC-HVDC links. In [12], a harmonic-based pilot protection scheme is presented for VSC-HVDC grids, which utilizes HHT for detecting transients. HHT, puts one step further than DWT, and gives information in time-instant frequency domain [13]. Based on the principle of instant frequency, initial peaks are accurately detected. However, HHT also needs high computation due to having complex mathematical operations. Considering the crucial needs for an ultra fast protection method in VSC-HVDC systems, neither HHT nor DWT can give practically fast and accurate results.

Other than the aforementioned literature works, comprehensive review of fault detection and localization algorithms for VSC-HVDC is given in [14,3].

Mathematical Morphology (MM), is a signal-processing method, which has been used for image-processing. It takes the advantage of morphing method for analyzing two-dimensional signals [15,16]. MM is based on combination of different operators, which can result in new methods with different behaviors in the accuracy and speed. The one-dimensional version of MM has been recently adopted for different power system analysis topics. As on some of the relevant literature works, authors in [17], used morphological filters to identify current transformer saturation. In [18], MM-based filters are used to detect power quality disturbances. In this paper, a series of mathematical morphology (MM)-based operators and filters are used for detecting fault TWs in VSC-HVDC links. The main contribution of this paper is to adopt MM for fault localization in VSC-HVDC grids, which solves the drawbacks of the referred literature studies. Accordingly, the contribution of this paper can be summarized as follow:

- This paper proposes MM-based fault location for VSC-HVDC links. Novel MM-based fault detection, with faster and more accurate results for VSC-HVDC links is studied.
- A variety of MM-based operators are analyzed for fault location. Analysis and validation of several MM operators is tested for VSC-HVDC links.
- Application of MM for high-impedance faults is studied.
- The ability of detecting the faulty pole for different MM operators is analyzed.
- The ability of different MM operators for detecting the second and the third TW reflections is studied.
- The proposed method is valid for VSC-HVDC links with different converter topologies.
- The method is applicable to both OHL and cable transmission.

- The method is accurate when multiple cable joints or different cable sections are used in deep and shallow parts of the ocean.
- There is no need for communication. Accordingly, no possible loss of data or communication delay exist.
- Due to having robust MM-based de-noising filters, the method is accurate in the noisy environment. De-noising filters also help the algorithm to distinguish between local TW reflections and TW reflections from the other side, which is of significant importance in single-ended TW-based fault localization.
- Impact of different parameters like the size and type of the structuring element (SE) is studied.
- A comprehensive discussion regarding the challenges and study topics for designing MM-based fault locators is given.

CIGRE DCS1 VSC-HVDC model is used in PSCAD/EMTDC and the MM-based signal processing is investigated in MATLAB. A number of faults with different characteristics, including high resistance faults are applied to the model to test the accuracy of the method. The remainder of this paper is organized as follows: The basics of TWs in VSC-HVDC links are explained in section II. MM operators and filters are comprehensively described in section III. Sections IV and V give the whole process and the simulation results, respectively. Finally, section VI and VII discuss different challenges and conclude the paper, respectively.

2 Traveling waves-Based Fault Location in VSC-HVDC Grids

The detection of TW reflections is a possible method for fault detection and localization in VSC-HVDC links. Fig. 1 shows a point-to-point VSC-HVDC link. As a fault happens in HVDC OHL or cable transmission, fault voltage and current waves propagate in both directions toward the busbars. When the TWs reach a different impedance from the transmission line, like a busbar in the substation at t_1^R, a portion of the waves reflect back toward the fault direction and a part of the waves continues forward propagation through new impedance path. When the reflected wave reaches the fault point again in t_{1F}^R, a part of the first reflection also reflects back again and reaches to the busbar for the second time t_2^R. A portion of the wave that is reflected back to the fault point, continues propagating in the backward direction and reaches to the other busbar in t_1^{RL}. This process continues until the waves are damped due to the line impedance.
Due to the existing coupling between the poles, modal transformation is used to have decoupled coaxial and ground modes, as given (1):

$$\begin{pmatrix} i_0 \\ i_1 \end{pmatrix} = \frac{1}{\sqrt{2}} \begin{pmatrix} 1 & 1 \\ 1 & -1 \end{pmatrix} \begin{pmatrix} I_p \\ I_n \end{pmatrix} \tag{1}$$

where, i_0 and i_1 are the coaxial and ground mode currents, respectively and I_p and I_n are the positive and negative mode currents, respectively. The

attenuation is different for OHLs and cables and the propagation speed also varies for different configurations of the transmission section. In summary, the modes are decoupled in high frequencies and the modal velocities remains almost constant at high frequencies [8]. Accordingly, in summary the propagation speed (modal velocity) for the coaxial mode can be determined using Eq. (1) [19]:

$$v_k = \frac{2\pi f}{i \operatorname{mag}(\Lambda_k)} \tag{2}$$

Where, v_k is the velocity for mode k, f is the frequency of cable parameter determination and Λ_k is the propagation constant for mode k. According to (2), which resulted from telegraph equations [20], the propagation speed is frequency-dependent and depends on the physical properties of the materials and also the layer configuration of the transmission section. The velocity of the Coaxial mode at high frequencies is about 280 m/us and for XLPE cables it is approximately 190 m/us [20].

According to the TW-based fault location methods, the location of the fault can be determined using either one-sided or two-sided measurement. Using the one-sided technique, the first arrival of the fault wave to the measurement point and the first reflection to the same point must be measured and the location will be determined using:

$$d = \frac{v(t_2^L - t_1^L)}{2} \tag{3}$$

When the two-sided measurement is used, a communication link is needed between two measurement points. The formulation for this method is given as:

$$d = \frac{v(t_1^L - t_1^R) + L_t}{2} \tag{4}$$

Both methods have good points and also drawbacks. In the two-sided measurement, only detection of the wavefront is needed. However, the communication delay can decrease the accuracy of the resulted location. The communication delay does not exist in the one-sided technique, but the detection of the second reflection is essential, which is a challenging task. According to Fig. 1, considering the left side measurements as the main criteria, it may be difficult for the left relay to distinguish between the propagation of reflection from the other end of the cable arriving at t_1^{RL} and the second reflection of the target wave arrived in t_2^L. This problem is more challenging in OHL transmission because of smaller attenuation compared to cable transmission.

3 Mathematical Morphology

The mathematical morphology (MM) is designed as a specific branch of mathematics, which is different from integral-transform based techniques [21]. The one-dimensional version of MM consists of modifying waveforms in the time domain using nonlinear signal filters. The main idea is to process the signals by a

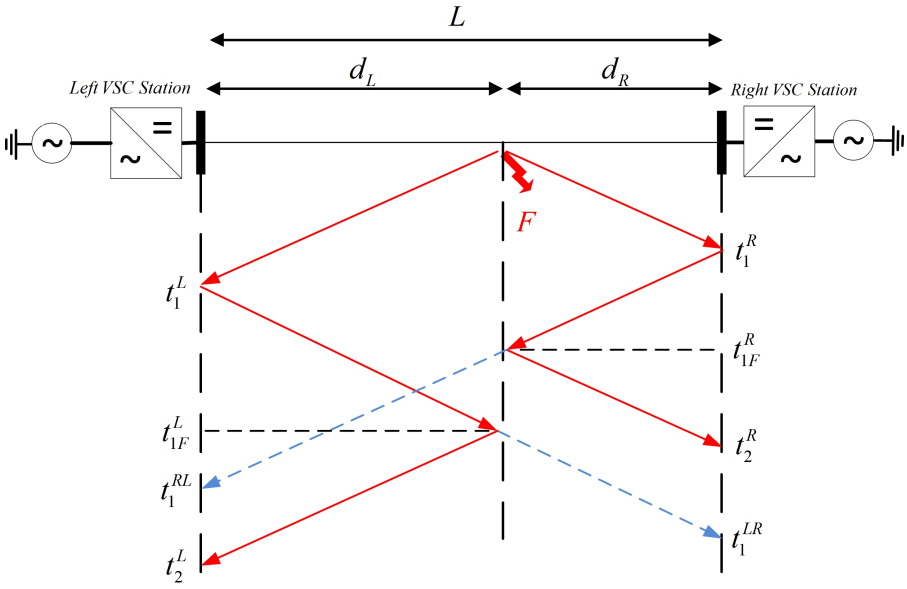

Fig. 1 Propagation of fault waves in VSC-HVDC transmission.

function named structuring element (SE) based on specific operators [22]. MM has a number of advantages over the other common signal-processing techniques used in power system fault detection as follows:

- MM depicts the signal profile directly in the time domain, which is different from other common methods like FT and WT transforms that analyze the signal in the frequency domain. Thereupon, it gives more accurate time information, while in FT there is no information regarding the time resolution and the time resolution information resulted from WT is not as accurate as MM results. Additionally, MM can be applied to non-periodic signals and detect different kinds of transients and disturbances.
- The process of MM is simpler than the usual methods. It is mainly due to simpler mathematical calculations compared to FT and WT, which must transform the signal into the frequency domain. MM operators do not use any multiplication or division during the signal-processing computations.
- The moving window used for sampling in MM can be significantly shorter than the window length used in WT and FT techniques. Additionally, it does not need high-sampling as WT for the detection of TWs in VSC-HVDC grids. This is particularly important for fault detection in VSC-HVDC transmission, which needs high-sampling due to the need for very fast fault isolation.
- MM is a flexible signal-processing technique that theoretically can detect every type of disturbance using the right adjustment of structuring element (SE) and the proper combination of MM-based operators and filters.

Table 1 Example 1: Dilation of input signal $f(n)$ using SE $g(m)$.

$f = [1.0, 1.2, 1.8, 1.1, 1.3, 1.5, 1.0, 1.4, 1.9]$
$g = [1, 0, 1]$
$\delta_g(0) = max(f(0) + g(0), f(-1) + g(1), f(-2) + g(2)) = max(2.0, -, -) = NA$
$\delta_g(1) = max(f(1) + g(0), f(0) + g(1), f(-1) + g(2)) = max(2.2, 1.0, -) = NA$
$\delta_g(2) = max(f(2) + g(0), f(1) + g(1), f(0) + g(2)) = max(2.8, 1.2, 2.0) = 2.8$
$\delta_g(3) = max(f(3) + g(0), f(2) + g(1), f(1) + g(2)) = max(2.1, 1.8, 2.1) = 2.1$
$\delta_g(4) = max(f(4) + g(0), f(3) + g(1), f(2) + g(2)) = max(2.3, 1.1, 2.8) = 2.8$
$\delta_g(5) = max(f(5) + g(0), f(4) + g(1), f(3) + g(2)) = max(2.5, 1.3, 2.1) = 2.5$
$\delta_g(6) = max(f(6) + g(0), f(5) + g(1), f(4) + g(2)) = max(2.0, 1.5, 2.3) = 2.3$
$\delta_g(7) = max(f(7) + g(0), f(6) + g(1), f(5) + g(2)) = max(2.4, 1.0, 2.5) = 2.5$
$\delta_g(8) = max(f(8) + g(0), f(7) + g(1), f(6) + g(2)) = max(2.9, 1.4, 2.0) = 2.9$
$\delta_g(f) = [N.A, N.A, 2.8, 2.1, 2.8, 2.5, 2.3, 2.5, 2.9]$

– MM gives accurate results when applied to noisy signals. Additionally, there are a number of MM-based de-noising filters that can be applied to the signal in real-time before processing the signal and facilitate the detection of transient peaks and disturbances easier from the de-noised wave.

Considering the above-mentioned advantages for MM techniques over traditional signal-processing methods used in protective relays, a new generation of protection algorithms are being developed for HVAC systems that can take the power system protection industry into the next generation [21]. This is particularly important for VSC-HVDC systems that need ultra-fast and accurate protection systems to have the minimum damage to the converter switches and a selective protection system for future multi-terminal connections. In this section, the basic MM operators, which can extract relevant structures of a set, are introduced first. Then, some of the proposed MM-based filters that can be used for noise filtering and fault analysis in VSC-HVDC grids are introduced.

3.1 Basic operators

In MM, Dilation and Erosion are the basic operators. Several filters and advanced operators are made using combinations of them. Considering $f(n)$ as the input signal and $g(m)$ as SE, dilation (δ_g) and erosion ($\in_g$) for the input signal $f(n)$ are determined as (5) and (6), respectively [23]:

$$\delta_g(f) = (f \oplus g)(n) - max \begin{cases} f(n-m) + g(m) \\ 0 \leq (n-m) \leq n, m \geq 0 \end{cases} \tag{5}$$

$$\in_g(f) = (f \oplus g)(n) - min \begin{cases} f(n+m) - g(m) \\ 0 \leq (n+m) \leq n, m \geq 0 \end{cases} \tag{6}$$

Examples of Dilation and Erosion for the input signal $f(n)$ and SE $g(m)$ are given in tables 1 and 2 , respectively.

Table 2 Example 2: Erosion of input signal $f(n)$ using SE $g(m)$.

$f = [1.0, 1.2, 1.8, 1.1, 1.3, 1.5, 1.0, 1.4, 1.9]$
$g = [1, 0, 1]$
$\in_g(0) = min(f(-2) - g(0), f(-1) - g(1), f(0) - g(2)) = min(-, -, 0.0) = NA$
$\in_g(1) = min(f(-1) - g(0), f(0) - g(1), f(1) - g(2)) = min(-, 1.0, 0.2) = NA$
$\in_g(2) = min(f(0) - g(0), f(1) - g(1), f(2) - g(2)) = min(0.0, 1.2, 0.8) = 0.0$
$\in_g(3) = min(f(1) - g(0), f(2) - g(1), f(3) - g(2)) = min(0.2, 1.8, 0.8) = 0.2$
$\in_g(4) = min(f(2) - g(0), f(3) - g(1), f(4) - g(2)) = min(0.8, 1.1, 0.3) = 0.3$
$\in_g(5) = min(f(3) - g(0), f(4) - g(1), f(5) - g(2)) = min(0.1, 1.3, 0.5) = 0.1$
$\in_g(6) = min(f(4) - g(0), f(5) - g(1), f(6) - g(2)) = min(0.3, 1.5, 0.0) = 0.0$
$\in_g(7) = min(f(5) - g(0), f(6) - g(1), f(7) - g(2)) = min(0.5, 1.0, 0.4) = 0.4$
$\in_g(8) = min(f(6) - g(0), f(7) - g(1), f(8) - g(2)) = min(0.0, 1.4, 0.9) = 0.0$
$\in_g(f) = [N.A, N.A, 0.0, 0.2, 0.3, 0.1, 0.0, 0.4, 0.0]$

Table 3 Example 3: Opening and Closing of input signal $f(n)$ using SE $g(m)$.

$f = [1.0, 1.2, 1.8, 1.1, 1.3, 1.5, 1.0, 1.4, 1.9]$
$g = [1, 0, 1]$
$\delta_g(f) = [N.A, N.A, 2.8, 2.1, 2.8, 2.5, 2.3, 2.5, 2.9]$
$\in_g(f) = [N.A, N.A, 0.0, 0.2, 0.3, 0.1, 0.0, 0.4, 0.0]$
$Op_g(f) = [N.A, N.A, N.A, N.A, 1.3, 1.2, 1.3, 1.4, 1.3]$
$Cl_g(f) = [N.A, N.A, N.A, N.A, 1.8, 1.1, 1.2, 1.5, 1.3]$

Other important MM operators are opening ($op_g(f)$) and closing ($cl_g(f)$), which are resulted from the conjugation of dilation and erosion operators, as follows [24]:

$$op_g(f) = f \circ g = (f \oplus g)(n) \ominus g \tag{7}$$

$$cl_g(f) = f \bullet g = (f \ominus g)(n) \oplus g \tag{8}$$

According to (7) and (8), opening corresponds to the dilation of the eroded signal and closing equals to the erosion of the dilated signal, respectively. Opening is generally used for smoothing the edges and peak noise, and closing is used for padding small holes [24]. Example of opening and closing of input signal $f(n)$ using SE $g(m)$ is given in table 3.

3.2 Structuring Element

Structuring element (SE) plays an important role in mathematical morphology-based signal processing. Voltage and current signal waves are one-dimensional and correspondingly a one-dimensional SE is used in MM. The length of SE and the SE elements can be defined by trial and error. However, there are specific typical values to start with them in power system studies [17]. SE commonly does not have a big size and the SE array values can be constant, increasing, decreasing, triangular, etc. The values are different according to the signal processing purpose, namely, filtering, disturbance or transient detection, etc. In this paper, the details of used SE for each case are given in section 5.

Table 4 Example 4: Morphological median de-noising filters of input signal $f(n)$ using SE $g(m)$.

$f = [1.0, 1.2, 1.8, 1.1, 1.3, 1.5, 1.0, 1.4, 1.9]$
$g = [1, 0, 1]$
$\Psi_1(f) = [N.A, N.A, 1.4, 1.15, 1.55, 1.3, 1.15, 1.45, 1.45]$
$\Psi_2(f) = [N.A, N.A, N.A, N.A, 1.55, 1.15, 1.25, 1.45, 1.3]$

3.3 Morphological Median Filter

There are various filters developed according to the basic MM operators for filtering the noise in several applications. Morphological median filter (MMF) is one of the common filters that give good results in analyzing power system fault signals [18]. MMF helps the protection system to distinguish the fault transients from the noise and short duration transients with a small amplitude. The main idea behind MMF is averaging the dilated and eroded signal to have the denoised waveform. It is the first MMF type ($\Psi_1(f)$), which is expressed by (9):

$$\Psi_1(f) = \frac{1}{2}(\delta_g(f) + \in_g(f)) \tag{9}$$

Another type of MMF can be defined as the average of opened and closed waveforms of a signal ($\Psi_2(f)$), given in (10):

$$\Psi_2(f) = \frac{1}{2}(op_g(f) + cl_g(f)) \tag{10}$$

3.4 Morphological Gradient

Other than de-noising filters, there are MM-based filters that can detect transients like power system fault events as feature extraction filters. For this purpose, two types of Morphological Gradient (MG) filters are defined as the subtraction of dilated and eroded signals ($\rho_1(f)$), as well as the difference between opened and closed waveforms ($\rho_2(f)$). They are defined in (11) and (12), respectively [18]:

$$\rho_1(f) = \delta_g(f) - \in_g(f) \tag{11}$$

$$\rho_2(f) = op_g(f) - cl_g(f) \tag{12}$$

A numerical example of morphological filtering is given in table 4.

3.5 Multi-Resolusion Morphological Gradient

Multi-resolution morphological gradient (MMG) is another tool that can accurately detect power system fault transients [25]. The main idea behind MMG is to have a scalable SE with different origins for detecting the ascending and descending edges of the fault transients. This concept can also detect the fault

direction and the faulty pole in the HVDC links. Two scalable SEs for each level are defined as (13) and (14):

$$g^{+} = \left\{ g_1, g_2, ..., g_{l-1}, \underline{g}_l \right\} \tag{13}$$

$$g^{-} = \left\{ \underline{g}_l, g_{l-1}, ..., g_2, g_1 \right\} \tag{14}$$

Where $\underline{g}_l$ is the origin of the SE and g^{+} and g^{-} are used for extracting ascending and descending edges of fault transients waveforms, respectively. According to (13) and (14), two SEs have inverted origins. Based on the defined ascending and descending SEs, MMG with decomposition level α is calculated as (15-17):

$$\rho^{\alpha}_{G^{+}} = \delta_{G^{+}}(\rho^{\alpha-1}) - \in_{G^{+}}(\rho^{\alpha-1}) \tag{15}$$

$$\rho^{\alpha}_{G^{-}} = \in_{G^{-}}(\rho^{\alpha-1}) - \delta_{G^{-}}(\rho^{\alpha-1}) \tag{16}$$

$$\rho^{\alpha} = \rho^{\alpha}_{G^{+}} + \rho^{\alpha}_{G^{-}} \tag{17}$$

3.6 Series Multi-Resolution Morphological Gradient

MMG has a great ability to extract transient components from the steady-state part of the signal. However, it can not accurately distinguish weak and slow transients. Thereupon, extending the MMG method by using β MMG operators in series order with similar or different SEs, as a series multi-resolution morphological gradient (SMMG) method, allows detecting weak transients accurately [17]. This will help detecting high-impedance or very short duration transients more accurately. In TW-based techniques, the detection of second reflections is significantly important when one-sided measurements are used. SMMG can significantly improve the accurate detection of the arrival time for wave reflections in VSC-HVDC links. In SMMG, a set of flat SEs are defined as $g_i, i = 1, 2, 3, ..., n$. The length os SEs are defined as $l_i = 2^{\alpha}_{i}$, where α_i is the MMG level with g_i as SE. In SMMG, at each order β, the signal is once passed through all levels of MMG_{α}. Thereupon, considering MMG_{α} as the multi-resolution morphological gradient at level α, operator $\mathrm{SMMG}^{\beta}_{\alpha}$ is defined as series multi-resolution morphological gradient in order β and at level α. Fig. 2 depicts the diagram of SMMG.

3.7 Generalized MMG

In the MMG method, the length of SE decreases dyadically. This way of defining SEs in MMG will result in having original SEs with long length. Using MMG may not have accurate results in capturing singular signals out of noise due to low efficiency in denoising. Accordingly, authors in [26] proposed a generalized MMG method (GMMG), in which the length of SE can successively increase or decrease with different certain rules, or even stay constant. In fact,

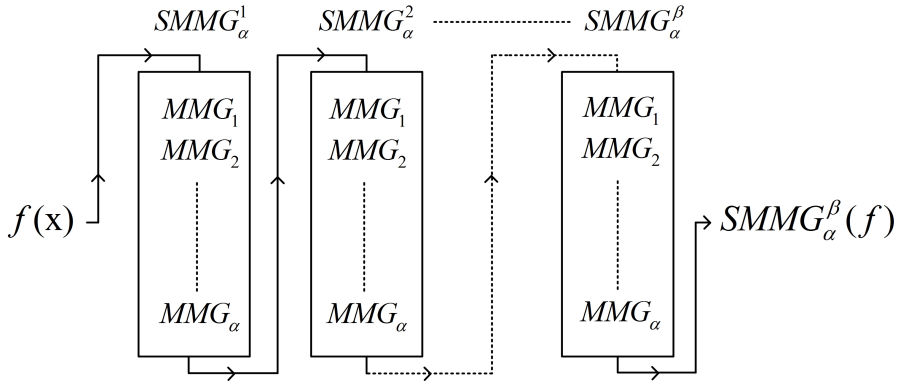

Fig. 2 Block diagram of SMMG applied to the input signal $f(x)$ with level α and order β.

all of the proposed MG-based methods are specific cases of GMMG. Using GMMG, the length of SE can be shortened and the best disturbance filtering and transient detection results can be achieved.

4 The whole Process

The whole process of fault detection and localization is depicted in Fig. 3. Each time the moving window is updated by one sample. During every processing step, both filters introduced in 9 and 10 are applied for de-noising the signal and detect the peaks more clearly. Then the selected MM filters are applied to the fault wave data. After the first peak detection, the algorithm starts to count the samples until detecting the second peak, which is the first reflected wave. Then the one-sided fault localization method is used based on (3) to determine the fault location.

In each sample, the fault current data in the moving window is used for morphing with the defined SE. The algorithm does the morphing process based on the combination of operators that are defined. The main inputs of the algorithm are the type and the size of SE, the fault peak setting, the moving window, the number of levels if multi-resolution morphology is used and the number of morphing orders if series MMG used. Accordingly, the algorithm is not sensitive to adjusting parameters, which results in a robust method for detecting faults in different situations and configurations.

In fault cases that the second peak is not detected, the algorithm cannot determine the fault and it is considered a failure in the fault detection. The detection of the third peak arrival is not considered in the process, due to not giving a reliable and accurate fault detection and localization.

In this study, every time that the simulation is run in PSCAD, the fault data from PSCAD plot window is copied as an input matrix in MATLAB for fault localization. Then, a 1024 sample moving window is defined in MATLAB, which will be updated by one sample in an outer loop. Inside the outer loop,

Table 5 CIGRE DCS1 system data

AC grid data	
AC Voltage (A1)	380 kV RMS line to line
AC Voltage (C1)	145 kV RMS line to line
SC level (B2 and B3)	30 GVA
R/X ratio	0.1
Converter data	
DC voltage control (Cm-A1)	+/- 200 kV
Reactive control (Cm-A1)	Qref=0 MVAR
Active power control (Cm-C1)	Pref= -400 MW
Reactive control (Cm-C1)	Qref=0 MVAR

firstly the de-noising filters are defined, and then an inner loop is defined, which covers the whole fault localization algorithm. In the inner loop, the morphological operators are defined and the fault localization is investigated. The input data are imported to the algorithm from an externally defined file.

5 Simulation Results

In this section, firstly the test model is explained and the defined case studies are presented. Then the results for each case are presented by figures and numerical tables. Each case study studies the impact of a specific parameter.

5.1 The test system

In this study, the CIGRE DCS-1 point-to-point VSC-HVDC link is modeled in PSCAD, which is shown in Fig. 4. The data for the CIGRE model and the converter control system description can be found in [27,28] and table 5. The sampling frequency is 20 kHz, which is generally considered a low sample rate in comparison with the sample rates used in some other researches. Several fault events are defined and applied to the model, which are given in table 6. MM-based Scripts are written and then applied to the fault current waves in MATLAB. One-sided TW-based fault localization technique given in (3) is used to determine the fault location. The results for different cases are given in the next subsections.

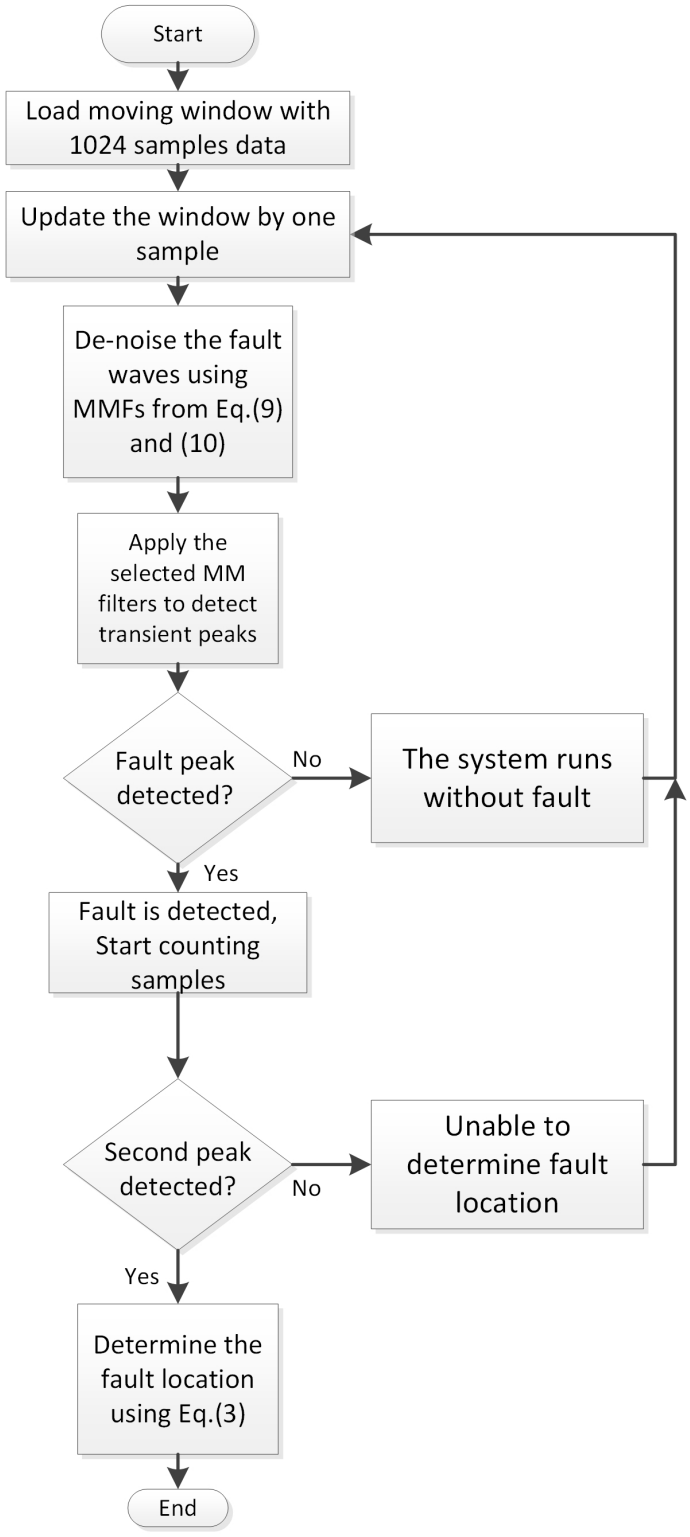

Fig. 3 The whole process for MM-based fault detection and localization.

Fig. 4 Single line diagram of CIGRE DCS1 VSC-HVDC link.

Table 6 Defined fault cases for different studies.

Fault No.	**Case study**	**Study topic**	**Fault type**	**Fault impedance** [Ω]	**Fault location** [**km**]
I	A	Impact of fault location	PP2G	0.1	50
II			PP2G	0.1	10
III			PP2G	0.1	90
IV	B	Impact of fault impedance	P2P	1	50
V			P2P	10	50
VI			P2P	50	50
VII			P2P	100	50
VIII	C	Impact of fault type	PP2G	0.1	50
IX			P2P	0.1	50
X			NP2G	0.1	50
XI	D	Impact of SE size	PP2G	0.1	50
XII	E	Impact of SE type	P2P	100	50

5.2 Case A: Impact of fault location

In this case, three low-impedance positive pole to the ground faults with the impedance of 0.1 Ω are applied to different locations from the right busbar at 1.63 [s]. A flat SE with a length of 30 elements and a value of 0.1 is used for MG. In the MMG method, two levels of multi-resolution morphological gradient MMG_2 are applied to the fault wave with the SE length of 8 for both ascending and descending SEs. Fig. 5(a) shows the fault wave diagram for the positive pole current measured on the right converter side for fault I. Using the MG filter, the detected peak arrivals are given in Fig. 5(b) and the results based on MMG_2 filter are given in Fig. 5(c). Fault location is determined using one-sided formulation given in (3) and the results are given in Table 7. Based on the table, The first, second and third peak detections for MG are 1.63032, 1.63077 and 1.63126 [s] for MG, respectively. Accordingly, the fault location of 45.5 [km] with the error of 9% is resulted. When MMG is used, the first, second and third peak detection values of 1.63035, 1.630965 and 1.63191 [s] detected. Accordingly the MMG-based fault location result is 47.7 [km], which results in 4.6% error. The results for faults II are 9.5 [km] and 10.45 [km] using MG and MMG, receptively, which gives the relative absolute errors of 5% and 4.5% respectively. The results for faults III are 3.44% and 0.27% for MG and MMG, respectively.

Table 7 Detected arrival times and fault location results for Case I using MG and MMG_2.

Fault No.	Filter	First arrival [s]	Second arrival [s]	Third arrival [s]	Estimated location [km]	Error [%]
I	MG	1.63032	1.63077	1.63126	45.5	9
	MMG	1.63033	1.63086	1.6314	47.7	4.6
II	MG	1.63006	1.63016	1.63026	9.5	5
	MMG	1.63005	1.63016	1.63027	10.45	4.5
III	MG	1.63045	1.63143	1.63239	93.1	3.44
	MMG	1.63047	1.63142	1.63235	90.25	0.27

According to the results, MMG_2 gives a more accurate location result than MG filters. Additionally, the detection of the second peak is more challenging for MG, which is clearly visible in Fig. 5(b). When MG filter is used, all detected peaks have positive values, which is not proper for the detection of the faulty pole. In MMG_2 the second peak has a negative value, which was expected because of using two inverted SEs to detect ascending and descending edges separately. Both methods have detection delays due to the difference in the sample numbers between the original wave and the filtered signals. In fact, this difference is because of multi-level dilation and erosion filters for MMG_2 and also for one level of dilation, erosion, opening and closing filters for MG.

5.3 Case B: Impact if fault impedance

In the second case study, faults with different impedances are applied to the middle of the transmission section. MMG_2 and $SMMG_2^3$ filters are used for detecting the fault TWs. The same SE as used for MMG_2 in case I is used for both MMG_2 and $SMMG_2^3$ in this case. Fig. 6 depicts the wave diagrams for this case study and the determined results are given in table 8. Based on the table, for fault VII, which is a 100 Ω fault and the most challenging case to detect, the first and the third peak detections for MMG_2 is 1.630335 and 1.63194 [s], while the second peak is not detected. When $SMMG_2^3$ used, the first, second and third peak detection times of 1.63033, 1.63086, and 1.6314 [s] detected. Accordingly, the estimated location using $SMMG_2^3$ is 47.7 [km], which leads to 4.6 % error.
According to Fig. 6(a), the high-impedance fault wave has more smooth and less sharp reflections than the low-impedance faults. Hence, the detection of arrived peaks is more challenging for high-impedance faults. It can be seen from Fig. 6(b) that the detection of the second fault wave peak, which is supposed to be in the green rectangular area, is not possible using MMG_2. As seen in Fig. 6(c), and Table 8, $SMMG_2^3$ can accurately detect the reflections. However, $SMMG_2^3$ cannot detect the direction and polarity of the fault. It is mainly because $SMMG_2^3$ is applied on the signal after being processed by MMG_2 and it will detect both ascending and descending points from the wave resulted from MMG_2 in Fig. 6(b). Thereupon, the second peak is detected with a positive value.

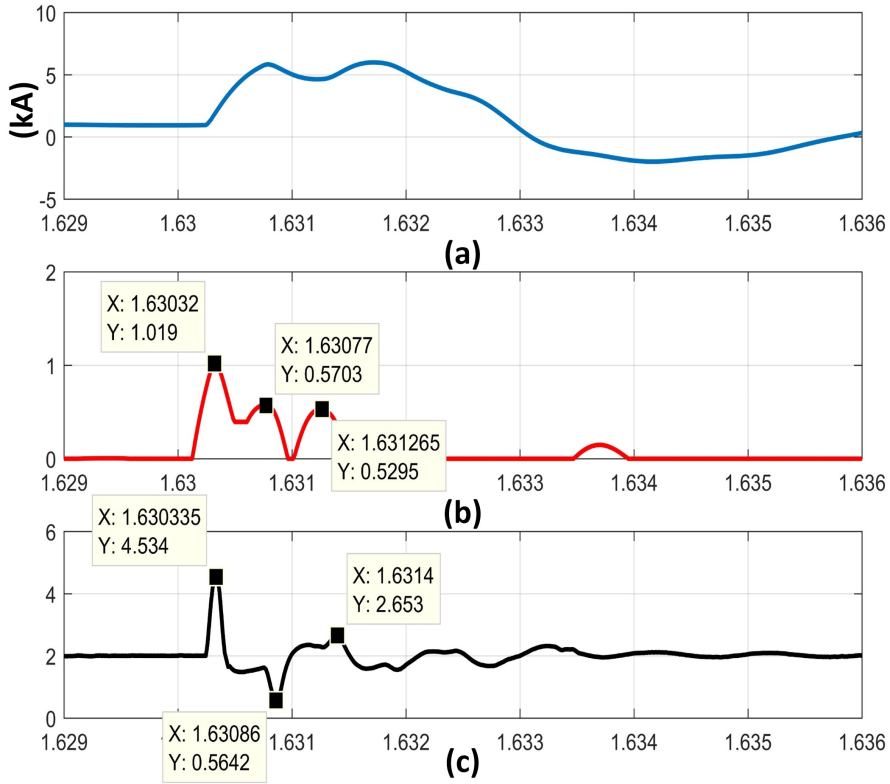

Fig. 5 Fault wave diagrams measured in the right positive pole for fault I of case study A. (a): original current wave, (b): peak detection results using MG (c): peak detection results using MMG_2

Table 8 Detected arrival times and fault location results for Case study B using MMG_2 and SMMG_2^3.

Fault No.	Filter	First arrival [s]	Second arrival [s]	Third arrival[s]	Estimated location[km]	Error [%]
IV	MMG_2	1.63032	1.63086	1.6312	51.3	2.6
	$SMMG_2^3$	1.63038	1.63095	1.6314	51.3	2.6
V	MMG_2	1.63036	-	1.63194	-	-
	$SMMG_2^3$	1.63037	1.630943	1.6315	51.6	3.2
VI	MMG_2	1.63035	-	1.63193	-	-
	$SMMG_2^3$	1.63036	1.630937	1.6315	52.0	4.0
VII	MMG_2	1.630335	-	1.63194	-	-
	$SMMG_2^3$	1.63035	1.63096	1.63191	47.7	4.6

Based on table 8, MMG_2 can only detect fault IV, which has impedance of 0.1 Ω. For faults V, VI and VII, which have higher impedances, the second peak is not detected. Accordingly, the fault location can not be determined. However, all faults in this case are detected using SMMG_2^3 with relative absolute error of 2.6%, 3.2%, 4.0% and 4.6%, respectively.

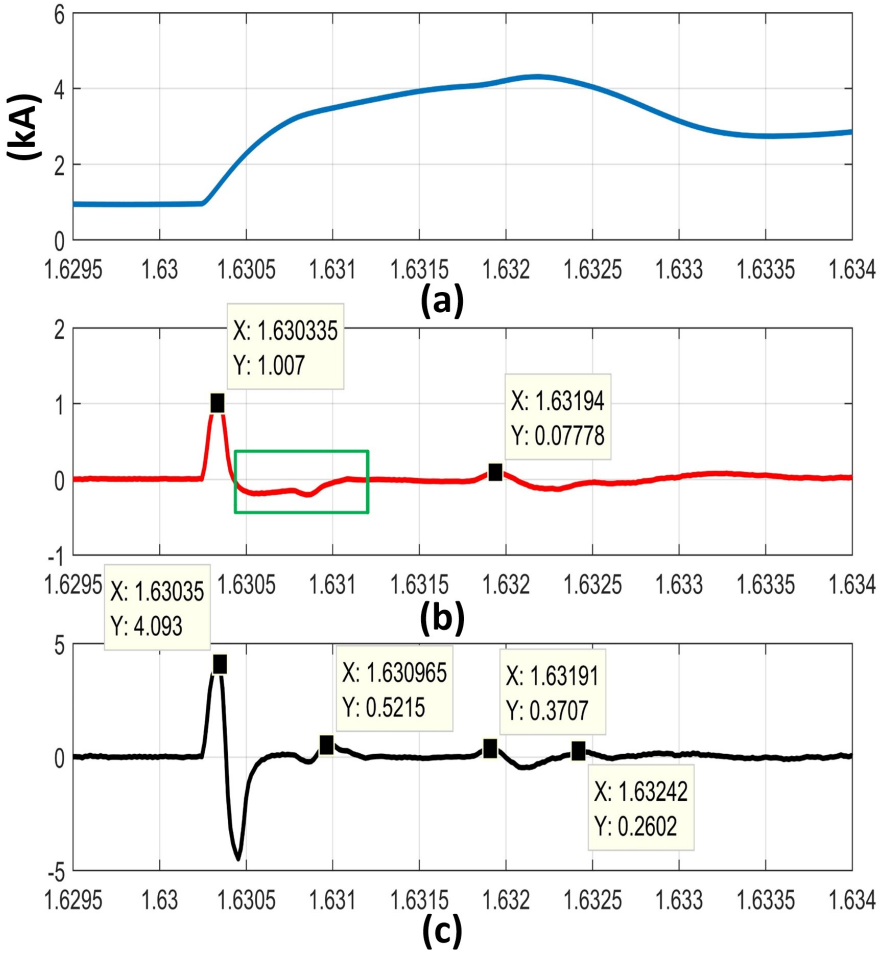

Fig. 6 Fault wave diagrams measured in the right positive pole for fault VII of Case study B. (a): original current wave, (b): peak detection results using MMG_2 (c): peak detection results using $SMMG_2^3$.

5.4 Case C: Impact of fault type

In this case study, three different fault types are applied to the model, which have the impedance of 0.1 Ω and are applied in the middle of the transmission section. Table 9 gives the results for this case study. According to the table 9, $SMMG_2^3$ can accurately detect fault location with different types. The relative absolute errors are 4.4%, 2.6% and 0.8% for PP2G, P2P and NP2G, namely faults VIII, IX and X, respectively.

Table 9 Detected arrival times and fault location results for Case study C using $SMMG_2^3$.

Fault No.	First arrival [s]	Second arrival [s]	Third arrival[s]	Estimated location[km]	Error [%]
VIII	1.63034	1.63092	1.6319	52.2	4.4
IX	1.63037	1.63094	1.6318	51.3	2.6
X	1.63038	1.63094	1.6310	50.5	0.8

5.5 Case D: Impact of SE size

In this case, different sizes of SE are used to detect the fault transients used in fault I using MMG_2. Fig. 7(a) shows the same original fault wave as fault I showed in Fig. 5(a). Fig. 7(b) to Fig. 7(d), depict the results of the transient detection using MMG_2 with SE size 8, 16 and 32, respectively. According to the results, increasing the size of SE does not necessarily increase the accuracy of the results. The main drawback of bigger size SEs is the increased sampling delay due to the morphology-based computations. Although the major peaks will be detected more clearly, smaller peaks are not clearly visible a using big size SE. Thereupon, using smaller SE size (in this case SE= 8) is chosen as the optimal size for detecting the fault. This size of SE will increase the computation speed due to resulting in shorter dilation and erosions.

5.6 Case E: Impact of SE type

In this case, fault detection results for fault VII are compared between MMG_2 and GMMG with two different types of SEs. In MMG, SE is bigger at first, and the size is divided after each level. While in GMMG, original SE has a smaller size and its length increases after each level. In this case, the original SE length of 8 and 2 are chosen for MMG_2 and GMMG, respectively. Fig. 8 depicts the corresponding wave diagrams. According to the figure, GMMG can detect the second reflection as well as results from SMMG. Additionally, it has the advantage of detecting the fault direction and thus can be used to detect the faulty pole. Moreover, due to using small SEs on the first level, the relay mathematical computations will be simpler in normal system operation when there is no fault event.

6 Discussion

The application of MM filters studied in section 5 and the resulted fault locations for different cases analyzed. The results, prove the feasibility and potential of MM-based fault locators. However, there are challenges in the accurate determination of the fault locations, which need special care, summarized as follows:

– When the transmission cable is long, due to the modal attenuations, the TW peak arrivals may not have a big amplitude, which makes the detection

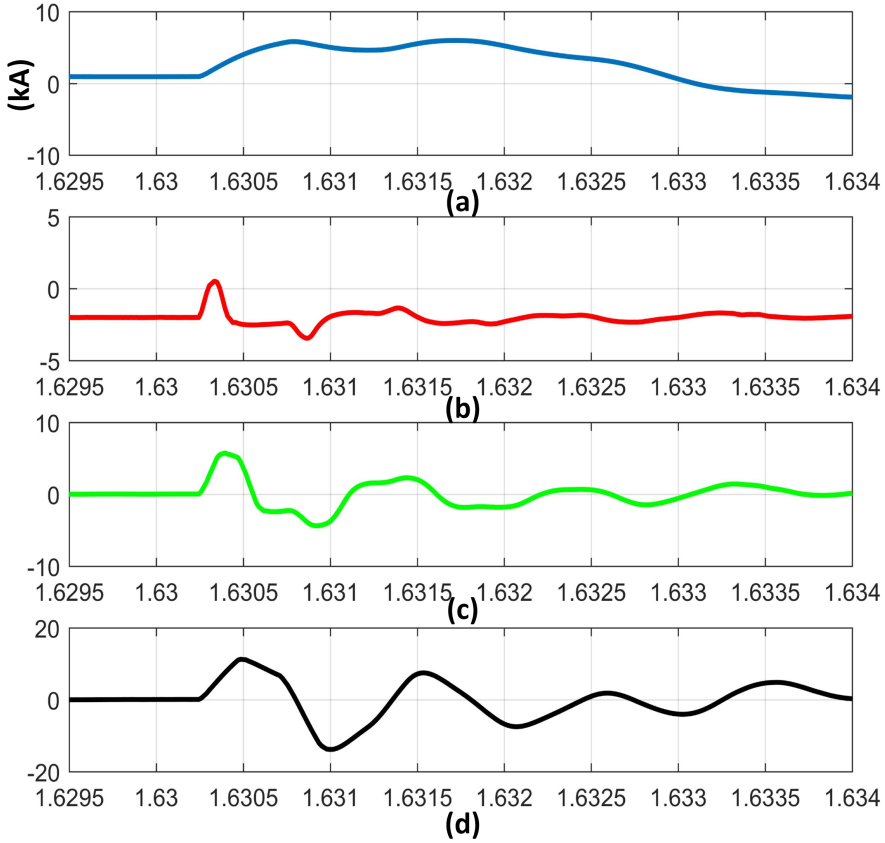

Fig. 7 Impact of SE size on transient detection of case study D and fault I using MMG_2. (a): original current wave, (b): peak detection results with SE size= 8 (c): peak detection results with SE size= 16 (d): peak detection results with SE size= 32.

of fault current peaks challenging. It will be more severe for the second and third peak arrivals. Additionally, between the second and the third arrivals, the converter may reach its blocking time threshold and consequently, there may not be any third reflections arriving at the relay location.

- HVDC cables may have some joints along the transmission sections, which are terminated. Additionally, there are cable terminations on the two sides of the cables. Accordingly, the impact of cable termination on the TW peak arrivals should be investigated [8].
- Errors in the measurement sensors may be common in HVDC voltage and current measurements, due to the need for high-sampling devices. Thereupon, the impact of measurement sensors on the MM-based fault locators must be tested.
- One of the important things to consider is the possibility of MM-based fault locators for multi-terminal VSC-HVDC (VSC-MTDC) grids. The

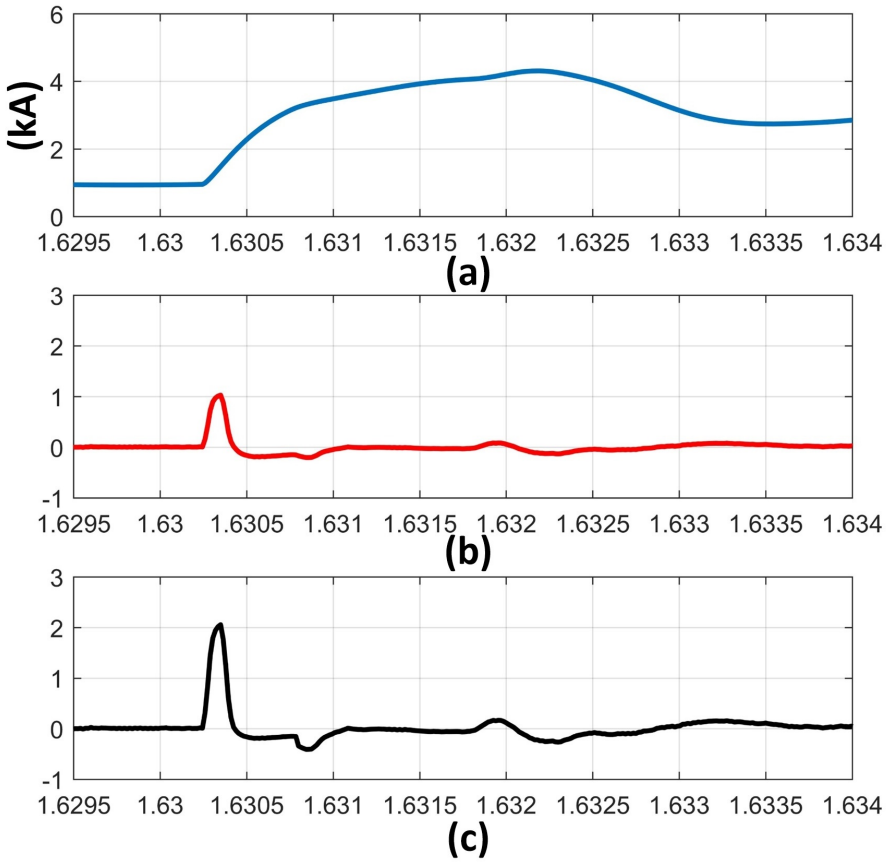

Fig. 8 Impact of SE type for case study E and fault VII using MMG_2 and GMMG (a): original current wave, (b): peak detection results using MMG_2 (c): peak detection results using GMMG.

important thing to care about is the complexity of reflections and refractions in different busbars in multi-terminal schemes. In these cases, robust combined MM-based filters with the ability to detect the fault direction and the faulty pole are suggested.

6.1 Comparison with literature works

In this subsection, a comparison of the detection time delay with literature works is presented. Table 10 gives the comparison details. Since no equal fault scenarios exist between a clear comparison, the average time delay of the proposed morphological-based methods is used for comparison. Additionally, the relative absolute error for the determined fault location between the methods is compared.

Table 10 Comparison of detection delay time with other literature studies.

Ref.	Used Method	Detection Delay (ms)	DCCB Delay	Relative Error	Considerations
[29]	ANN	4.5	√	1.16	26 ms delay in fault localization
[30]	DWT	2.375	-	5.54	Tested only for two-level VSC-MTDC
[31]	TW	5	√	-	Operating time for DCCB is included
[32]	Transient	1.74	-	3.35	Different delay values for different faults
[33]	S-transform	2	-	3.56	1 ms must be added for com. delay
[34]	TW	3	√	2.92	DWT used for peak detection
[35]	ROCOV	0.2	-	4.5	2 ms for DCCB must be added
[36]	Transient	1	-	4.0	Distributed optical sensors are used
MG	TW	**2.21**	√	3.44-5	
MMG	TW	**2.19**	√	3.4-4.5	
SMMG	TW	**2.13**	√	0.8-2.6	
GMMG	TW	**2.09**	√	0.5	

7 Conclusions

In this paper, the application of MM filters for detecting fault transients in VSC-HVDC links has been studied. Multiple filters have been analyzed based on the basic MM operators and applied to different fault cases to extract TW peak arrivals from the fault current waves. The results validated the accuracy of the MM-based fault locators with concluding remarks as follows:

- It has resulted that MM-based fault locators locate the faults with minimum error for both low and high-impedance faults.
- Both MG and MMG can locate the fault. However, among MG and MMG filters, MMG with two levels of gradient (MMG_2) gives more accurate results. MMG gave the relative absolute error of 0.27% at it's best, while MG gave 3.44%.
- In case of high-resistance faults, MMG_2 can not detect the second reflections accurately, while SMMG_2^3 can detect the second and third reflections accurately. On the other hand, SMMG_2^3 can not detect the faulty pole, while it is possible in MMG_2.
- For high-resistance faults, the accuracy of SMMG_2^3 is between 3.2% and 4.6%, while MMG_2 cannot detect the high-resistance faults.
- It has resulted that GMMG has both advantages of detecting second and third reflections in different fault types, and the fault direction and pole, which was not possible in SMMG_2^3. GMMG also has the advantage of using short SE in the beginning, which significantly lightens the MM-based algorithm process in non-faulty and steady-state system conditions.
- Increasing SE size, not always increase the accuracy, but also leads to more sample delays in locating the fault. Bigger SE will make the high transient peaks sharper and easier to detect, while small transients will not be clearly detected. Accordingly, moderate size of SE should be used to have a trade-off between the accuracy and sample delay.
- A proper selection of SE in the GMMG method gave the best results with more simple computation and directional information.

- Regarding the average sample delay values, MG, MMG and SMMG result in 0.21 ms, 0.19 ms and 13 ms, while GMMG resulted in the fastest detection with 0.9 ms delay.
- Comparing with literature works, GMMG gave the detection delay of 0.09 ms, which is less than a majority of results in the literature works.
- According to many possibilities in combining MM filters, the flexibility of the method to the type and size of SE, and with the introduction of generalized MMG, theoretically, every kind of disturbance can be accurately detected with proper selection of filters and SE.

Further work can be consisted of applying the MM-based fault detection and localization technique to multi-terminal VSC-HVDC transmission systems in order to test the ability of the method in selective fault detection and accurate localization in more complicated grids. Due to scalability of the proposed method, it can be extended to the grids with other voltage levels, such as medium voltage DC (MVDC) and low voltage DC (LVDC) grids. The method can also be extended to LCC-HVDC transmission links.

References

1. Y. Yang and C. Huang, "A single-ended fault location method for DC lines in bipolar MMC-HVDC system," *Electrical Engineering*, jan 2020.
2. B. Chang, O. Cwikowski, M. Barnes, R. Shuttleworth, A. Beddard, and P. Coventry, "Review of different fault detection methods and their impact on pre-emptive vsc-hvdc dc protection performance," *High Voltage*, vol. 2, no. 4, pp. 211–219, 2017.
3. M. Ashouri, C. L. Bak, and F. F. D. Silva, "A review of the protection algorithms for multi-terminal vcd-hvdc grids," in *2018 IEEE International Conference on Industrial Technology (ICIT)*, 2018, pp. 1673–1678.
4. N. Halem, A. Rajapakse, "Local measurement based ultra-fast directional ROCOV scheme for protecting Bi-pole HVDC grids with a metallic return conductor," *Electric Power and Energy Systems*, vol. 98, pp. 323–330, 2018.
5. S. Azizi, M. Sanaye-Pasand, M. Abedini, and A. Hassani, "A traveling-wave-based methodology for wide-area fault location in multiterminal DC systems," *IEEE Transactions on Power Delivery*, vol. 29, no. 6, pp. 2552–2560, dec 2014.
6. J. Liu, N. Tai and . Fan, "Transient-Voltage-Based Protection Scheme for DC Line Faults in the Multiterminal VSC-HVDC Systems," *IEEE Transactions on Power Delivery*, vol. 32, no. 3, pp. 1483–1494, 2017.
7. A, Elanien, A. Elserougi, A. Abdel-Khalik, A. Massoud, and S. Ahmed, "A differential protection technique for multi-terminal HVDC," *Electric Power Systems Research*, vol. 130, no. 1, pp. 78–88, 2016.
8. M. Ashouri, F. F. D. Silva, and C. L. Bak, "On the application of modal transient analysis for online fault localization in HVDC cable bundles," *IEEE Transactions on Power Delivery*, pp. 1–1, 2019.
9. M. Daisy, R. Dashti, and H. R. Shaker, "A new fault-location method for HVDC transmission-line based on DC components of voltage and current under line parameter uncertainty," *Electrical Engineering*, vol. 99, no. 2, pp. 573–582, jul 2016.
10. L. Sabug, A. Musa, F. Costa, and A. Monti, "Real-time boundary wavelet transform-based DC fault protection system for MTDC grids," *International Journal of Electrical Power & Energy Systems*, vol. 115, p. 105475, feb 2020.
11. M. Ashouri, F. F. da Silva, and C. L. Bak, "Online fault location in monopolar LCC-HVDC links with metallic return using modal transient data," in *2019 IEEE International Conference on Environment and Electrical Engineering and 2019 IEEE Industrial and Commercial Power Systems Europe (EEEIC / I&CPS Europe)*. IEEE, jun 2019.

12. M. Ashouri, F. F. da Silva, and C. L. Bak, "A harmonic based pilot protection scheme for VSC-MTDC grids with PWM converters," *Energies*, vol. 12, no. 6, p. 1010, mar 2019.
13. M. V.Kazemi, S. J. Sadati, and S. A. Gholamian, "Adaptive frequency control support of a DFIG based on second-order derivative controller using data-driven method," *International Transactions on Electrical Energy Systems*, vol. 30, no. 7, p. 2050-7038, mar 2019.
14. B. Li, J. He, Ye Li and B. Li, "A review of the protection for the multi-terminal VSC-HVDC grid," *Protection and Control of Modern Power Systems*, vol. 4, no. 1, 2019.
15. J. Goutsias and H. J. A. M. Heijmans, "Nonlinear multiresolution signal decomposition schemes. i. morphological pyramids," *IEEE Transactions on Image Processing*, vol. 9, no. 11, pp. 1862–1876, 2000.
16. H. J. A. M. Heijmans and J. Goutsias, "Nonlinear multiresolution signal decomposition schemes. ii. morphological wavelets," *IEEE Transactions on Image Processing*, vol. 9, no. 11, pp. 1897–1913, 2000.
17. X. Lin, L. Zou, Q. Tian, H. Weng, and P. Liu, "A series multiresolution morphological gradient-based criterion to identify ct saturation," *IEEE Transactions on Power Delivery*, vol. 21, no. 3, pp. 1169–1175, 2006.
18. Z. Lu, D. R. Turner, Q. H. Wu, J. Fitch, and S. Mann, "Morphological transform for detection of power quality disturbances," in *2004 International Conference on Power System Technology, 2004. PowerCon 2004.*, vol. 2, 2004, pp. 1644–1649 Vol.2.
19. A. Ametani, T. Ohno, and N. Nagaoka, *Cable System Transients: Theory, Modeling and Simulation (Wiley - IEEE)*. Wiley-IEEE Press, 2015.
20. F. F. da Silva and C. L. Bak, *Electromagnetic Transients in Power Cables (Power Systems)*. Springer, 2013.
21. Q. Wu, Z. Lu, and T. Ji, *Protective Relaying of Power Systems Using Mathematical Morphology*. Springer, 2009.
22. L. Zou, P. Liu, and Q. Zhao, "Mathematical morphology based phase selection scheme in digital relaying," *IEE Proceedings - Generation, Transmission and Distribution*, vol. 152, no. 2, pp. 157–163, 2005.
23. S. Gautam and S. M. Brahma, "Overview of mathematical morphology in power systems: A tutorial approach," in *2009 IEEE Power Energy Society General Meeting*, 2009, pp. 1–7.
24. G. Li, M. Zhou, Y. Luo, and Y. Ni, "Power quality disturbance detection based on mathematical morphology and fractal technique," in *2005 IEEE/PES Transmission Distribution Conference Exposition: Asia and Pacific*, 2005, pp. 1–6.
25. Q. H. Wu, J. F. Zhang, and D. J. Zhang, "Ultra-high-speed directional protection of transmission lines using mathematical morphology," *IEEE Power Engineering Review*, vol. 22, no. 11, pp. 54–54, 2002.
26. X. Lin, H. Weng, H. Liu, W. Lu, P. Liu, and Z. Bo, "A novel adaptive single-phase reclosure scheme using dual-window transient energy ratio and mathematical morphology," *IEEE Transactions on Power Delivery*, vol. 21, no. 4, pp. 1871–1877, 2006.
27. T. Vrana, S. Dennetiere, Y. Yang, J. Jardini, D. Jovcic, and H. Saad, "The cigre b4 dc grid test system," vol. 270, 10 2013.
28. R. Irnawan, F. F. da Silva, C. L. Bak, and T. C. Bregnhøj, "A categorization of converter station controllers within multi-terminal dc transmission systems," in *2016 IEEE/PES Transmission and Distribution Conference and Exposition (T D)*, 2016, pp. 1–5.
29. Q. Yang, S. Blond, R. Aggarwal, Y. Wang, J. Li, "New ANN method for multi-terminal HVDC protection relaying,", Electric Power System Research, 2016, pp. 192–201.
30. Kerf, K.D.; Srivastava, K.; Reza, M.; Bekaert, D.; Cole, S.; Hertem, D.V.; Belmans, R. Wavelet-based protection strategy for DC faults in multi-terminal VSC HVDC systems. *IET Gener. Transm. Distrib.* **2011**, *5*, 496. doi:https://doi.org/10.1049/iet-gtd.2010.0587.
31. Mobarez, M.; Kashani, M.G.; Chavan, G.; Bhattacharya, S. A novel control approach for protection of multi-terminal VSC based HVDC transmission system against DC faults. In Proceedings of the 2015 IEEE Energy Conversion Congress

and Exposition (ECCE). IEEE, Montreal, QC, Canada, 20–24 September 2015; doi:https://doi.org/10.1109/ecce.2015.7310254.
32. Liu, J.; Tai, N.; Fan, C. Transient-Voltage-Based Protection Scheme for DC Line Faults in the Multiterminal VSC-HVDC System. *IEEE Trans. Power Deliv.* **2017**, *32*, 1483–1494.
33. Zhao, P.; Chen, Q.; Sun, K. A novel protection method for VSC-MTDC cable based on the transient DC current using the S transform. *Int. J. Electr. Power Energy Syst.* **2018**, *97*, 299–308. doi:https://doi.org/10.1016/j.ijepes.2017.11.007.
34. Zou, G.; Feng, Q.; Huang, Q.; Sun, C.; Gao, H. A fast protection scheme for VSC based multi-terminal DC grid. *Int. J. Electr. Power Energy Syst.* **2018**, *98*, 307–314. doi:https://doi.org/10.1016/j.ijepes.2017.12.022.
35. Haleem, N.M.; Rajapakse, A.D. Local measurement based ultra-fast directional ROCOV scheme for protecting Bi-pole HVDC grids with a metallic return conductor. *Int. J. Electr. Power Energy Syst* **2018**, *98*, 323–330. doi:https://doi.org/10.1016/j.ijepes.2017.11.033.
36. Tzelepis, D.; Dyśko, A.; Fusiek, G.; Nelson, J.; Niewczas, P.; Vozikis, D.; Orr, P.; Gordon, N.; Booth, C.D. Single-Ended Differential Protection in MTDC Networks Using Optical Sensors. *IEEE Trans. Power Deliv.* **2017**, *32*, 1605–1615.